

Using the sound-proof limit for balanced data initialization

Rupert Klein, Tommaso Benacchio, Warren O’Neill

*FB Mathematik & Informatik, Freie Universität Berlin
Arnimallee 6, 14195 Berlin, Germany
rupert.klein@math.fu-berlin.de*

ABSTRACT

There is substantial theoretical evidence that the pseudo-incompressible model (Durrán 1989) is a valid approximation to the equations of fully compressible flow in meso-scale atmospheric flow regimes. Arguably, numerical methods for the integration of the compressible flow equations should then produce essentially pseudo-incompressible results at low flow speeds if the initial data are acoustically balanced. This paper summarizes the construction of a compressible flow solver that observes this desirable. Given a pseudo-incompressible solver, the design of the scheme requires little additional coding as it exploits the close structural similarity of the compressible and pseudo-incompressible model equations.

The modified scheme allows us to solve the compressible, pseudo-incompressible, and a continuous family of intermediate models, all of which conserve a model-dependent total energy. We conjecture that such a continuous transition from the full dynamics to a balanced model can be utilized for balanced data assimilation.

1 Introduction

Although dynamical cores based on the compressible flow equations have become standard in today’s regional weather forecasting codes, the development of refined time discretizations remains an area of active research, see, e.g., [Tanguay et al. \(1990\)](#); [Wicker and Skamarock \(2002\)](#); [Reisner et al. \(2005\)](#); [Gatti-Bono and Colella \(2006\)](#); [Wensch et al. \(2009\)](#); [Durrán and Blossey \(2012\)](#); [Smolarkiewicz et al. \(2013\)](#); [Benacchio et al. \(2013\)](#). The task is challenging because of the simultaneous presence of a multitude of different atmospheric flow regimes that can be characterized through various distinguished limits involving the Mach-, Froude-, and Rossby-numbers and additional dimensionless parameters characterizing, e.g., moist air processes. The related asymptotic limit regimes constitute valuable points of reference in the construction and validation of numerical discretizations of the full compressible dynamics ([Klein \(2000\)](#); [Cullen \(2007\)](#)). Subscribing to this program, we consider here the asymptotic design regime for the class of “sound-proof models”, which include the anelastic ([Ogura and Phillips \(1962\)](#); [Dutton and Fichtl \(1969\)](#); [Lipps and Hemler \(1985\)](#); [Bannon \(1996\)](#)) and pseudo-incompressible ([Durrán \(1989\)](#)) equation sets.

In a previous ECMWF report ([Klein \(2011\)](#)) one of the present authors summarized recent theoretical arguments showing that the Lipps-Hemler anelastic and Durrán’s pseudo-incompressible models are asymptotically consistent with the compressible flow equations for realistic potential temperature stratifications found in the troposphere, for vertical scales comparable to the pressure scale height, and for horizontal meso-scales, see [Klein \(2009, 2010\)](#); [Klein et al. \(2010\)](#); [Klein and Pauluis \(2011\)](#) for detailed accounts. [Achatz et al. \(2010\)](#) showed that the pseudo-incompressible model also faithfully approximates breaking wave packets under stratification conditions typical for the stratosphere, while here the anelastic model solutions would deviate at leading order from the compressible dynamics. Encouraged by these results we argue that a discretization of the full compressible flow equations should asymptote to a discretization of the pseudo-incompressible model in the limit of slow flows and acoustically balanced initial data.

The point of departure for the developments in this paper are the non-dimensionalized inviscid compressible and pseudo-incompressible flow models written in conservation form for the mass, ρ , momentum, $\rho\vec{v}$, and potential temperature, $\rho\theta \equiv P$, densities, see Klein (2009),

$$\rho_t + \nabla \cdot (\rho\vec{v}) = 0 \quad (1)$$

$$(\rho\vec{v})_t + \nabla \cdot (\rho\vec{v} \circ \vec{v}) + P\nabla\pi = -\rho g\vec{k} \quad (2)$$

$$\alpha P_t + \nabla \cdot (P\vec{v}) = 0 \quad (3)$$

Here α is a switch that produces the pseudo-incompressible and compressible models for $\alpha = 0$ and $\alpha = 1$, respectively, provided we adopt the appropriate definition for the pressure variable π . In the pseudo-incompressible setting π acts as a Lagrange multiplier that guarantees compliance with the divergence constraint $\nabla \cdot (P\vec{v}) = 0$. In the compressible setting P and π are related to the thermodynamic pressure p by

$$P = p^{1/\gamma}, \quad \pi = \frac{p^\Gamma}{\Gamma} \quad \text{where} \quad \Gamma = \frac{\gamma-1}{\gamma}, \quad (4)$$

and γ is the isentropic exponent. Note that the potential temperature, θ , is defined by the two conserved variables P and ρ through

$$\rho\theta = P. \quad (5)$$

A straightforward calculation shows that the models in (1)–(3) satisfy total energy conservation laws

$$E_{\alpha,t} + \nabla \cdot ([E_\alpha + p_\alpha^*]\vec{v}) = 0, \quad (6)$$

where

$$E_\alpha = \frac{p_\alpha}{\gamma-1} + \rho \frac{\vec{v}^2}{2} + \rho gz, \quad (7)$$

$$p_\alpha = \alpha p + (1-\alpha)\bar{p} \quad (8)$$

$$p_\alpha^* = \frac{\gamma-\alpha}{\gamma-1}p - \frac{1-\alpha}{\gamma-1}\bar{p} \quad (9)$$

with $\bar{p}(z)$ the background pressure distribution of the limiting pseudo-incompressible model to which the thermodynamic pressure p converges as $\alpha \rightarrow 0$.

Interestingly, the energy conservation principle in (6) holds not only for the limiting models but also for all intermediate models. That is, for any $\alpha \in [0, 1]$ we have approximate models that are stable in the respective total energy norm. In the next section we discuss a numerical discretization that operates seamlessly for all these models.

2 Semi-implicit semi-discretization in time

The basis for the numerical integration of (1)–(3) is a second order accurate mid-point rule in time and a finite volume discretization in space. Thus we have, for the update from time step n to time step $n+1$,

$$\rho^{n+1} - \rho^n = -\Delta t \tilde{\nabla} \cdot (\rho\vec{v})^{n+\frac{1}{2}} \quad (10)$$

$$(\rho\vec{v})^{n+1} - (\rho\vec{v})^n = -\Delta t \left(\rho^{n+\frac{1}{2}} g\vec{k} + \tilde{\nabla} \cdot (\rho\vec{v} \circ \vec{v})^{n+\frac{1}{2}} - (P\tilde{\nabla}\pi)^{n+\frac{1}{2}} \right) \quad (11)$$

$$\alpha (P^{n+1} - P^n) = -\Delta t \tilde{\nabla} \cdot (P\vec{v})^{n+\frac{1}{2}} \quad (12)$$

For any control volume C in our cartesian mesh with a set of bounding interfaces \mathcal{I}_C we define the approximate divergence of a vector field \vec{f} as

$$\left(\tilde{\nabla} \cdot \vec{f}\right)_C = \frac{1}{|C|} \sum_{I \in \mathcal{I}_C} \vec{f}_I \cdot \vec{n}_I A_I \quad (13)$$

and the gradient of a scalar function g as

$$\left(\tilde{\nabla} g\right)_C = \frac{1}{|C|} \sum_{I \in \mathcal{I}_C} g_I \vec{n}_I A_I, \quad (14)$$

with A_I denoting the area of interface I and \vec{f}_I, g_I being the values of the functions \vec{f}, g evaluated at the centers of mass of the interfaces or the respective area averages.

2.1 Predictor-corrector scheme for the advective fluxes

As in Klein (2009) the advective fluxes are based on upwinding relative to a carrier flux $(P\vec{v})^{n+\frac{1}{2}}$. The carrier flux consists of an explicit prediction and a pressure-implicit correction, so that

$$(P\vec{v})^{n+\frac{1}{2}} = (P\vec{v})^{n+\frac{1}{2},*} - \frac{\Delta t}{2} (P\theta)^{n+\frac{1}{2},*} \nabla \delta \pi \quad (15)$$

where

$$\delta \pi = \pi^{n+1} - \pi^n. \quad (16)$$

Let us abbreviate (15) as

$$(P\vec{v})^{n+\frac{1}{2}} = (P\vec{v})^{n+\frac{1}{2},*} + \delta(P\vec{v}), \quad (17)$$

then the advective fluxes of the mass and momentum densities read

$$(P\vec{v}\phi)^{n+\frac{1}{2}} = (P\vec{v})^{n+\frac{1}{2},*} \phi_{\text{up}}^{n+\frac{1}{2},*} + \delta(P\vec{v}) \phi_{\text{up}}^{n+1,*} \quad (18)$$

where $\phi = 1/\theta$ for the mass flux and $\phi = v_i/\theta$ for the transport of the i th component of momentum with v_i the associated velocity component, and the subscript ‘‘up’’ indicates upwind evaluation at the cell interfaces from piecewise polynomial reconstructions of the solution data within the control volumes.

All explicit components of the numerical fluxes are labelled by the single asterisc superscript and are obtained in the course of solving an auxiliary equation system over one time step by an explicit finite volume scheme. The auxiliary system is identical to (1)–(3) for $\alpha = 1$, except that the pressure variable in the momentum equation is frozen at its old time level. With the pressure in the momentum equation decoupled in this fashion, the system no longer supports acoustic modes and the time step of an explicit scheme can be chosen based on an advective Courant number. The details of this step as used in generating the results presented below has been described in detail by Klein (2009) in the context of sound-proof model discretizations.

Of primary interest here is the pressure-implicit correction. Using (15) in the update of the energy variable, P , in (12) and approximating the time update of P by the time increment of the Exner pressure, $\delta \pi$, i.e., by

$$P^{n+1} - P^n = \left(\frac{dP}{d\pi}\right)^{n+\frac{1}{2}} \delta \pi, \quad (19)$$

we obtain

$$-\alpha \left(\frac{dP}{d\pi}\right)^{n+\frac{1}{2}} \frac{\delta \pi}{\Delta t} + \frac{\Delta t}{2} \tilde{\nabla} \cdot \left((P\theta)^{n+\frac{1}{2},*} \tilde{\nabla} \delta \pi\right) = \tilde{\nabla} \cdot (P\vec{v})^{n+\frac{1}{2},*} \equiv -\frac{1}{\Delta t} (P^{n+1,*} - P^n). \quad (20)$$

For $0 < \alpha \leq 1$ this is the Helmholtz-equation for pressure increments as encountered in similar second-order semi-implicit compressible schemes. The related literature is voluminous, but see, e.g., [Bijl and Wesseling \(1998\)](#); [Colella and Pao \(1999\)](#); [Munz et al. \(2003\)](#); [Reisner et al. \(2005\)](#); [Reich \(2006\)](#); [Restelli and Giraldo \(2009\)](#); [Jebens et al. \(2011\)](#); [Smolarkiewicz et al. \(2013\)](#) and references therein. For $\alpha = 0$ it reduces to the Poisson-type pressure equation as found in second- and higher-order projection methods, see, e.g., [Bell and Marcus \(1992\)](#); [Almgren et al. \(1996\)](#); [Schneider et al. \(1999\)](#); [Minion \(2003\)](#); [Almgren et al. \(2006\)](#) and references therein.

To complete the continuous blending of the sound-proof and compressible dynamics, a decision needs to be made as regards the pressure time update. In the sound-proof case, $\alpha = 0$, the situation is clear. We compute $\delta\pi = \pi^{n+1} - \pi^n$ from the Poisson equation and thus have the update of the pressure variable π readily available. In the fully compressible case, with $\alpha = 1$, we have two candidates for the final pressure update after solution of the Helmholtz-equation. The first is again $\delta\pi$, while the second is given by the conservative update of the energy equation, i.e., by $P^{n+1} - P^n$ from (12), combined with the equations of state in (4). We enforce a conservative update of the energy variable, P , in this case and choose the second option. For the intermediate cases, $0 < \alpha < 1$, we adopt a linear interpolation between the two, i.e.,

$$\pi^{n+1} = \pi^n + \alpha \left((P^{n+1})^{\gamma\Gamma} - (P^n)^{\gamma\Gamma} \right) + (1 - \alpha) \delta\pi. \quad (21)$$

2.2 Pressure gradient approximation for the momentum equation

The previous section described the calculation of advective numerical fluxes. Yet, the predicted momentum density, $(\rho\vec{v})^{n+1,*}$, was obtained using the pressure gradient from time level n only. This amounts to merely first-order accuracy and does not provide a stable scheme. By solving a second implicit pressure equation, we obtain here an update of the pressure gradient in the momentum equation, so that

$$(\rho\vec{v})^{n+1} = (\rho\vec{v})^{n+1,**} - \frac{\Delta t}{2} P^{n+\frac{1}{2},**} \bar{\nabla} \delta\pi, \quad (22)$$

where the pressure increment satisfies a discretization of the energy equation from (3) similar to (20),

$$-\alpha \left(\frac{dP}{d\pi} \right)^{n+\frac{1}{2},**} \frac{\delta\pi}{\Delta t} + \frac{\Delta t}{4} \bar{\nabla} \cdot \left((P\theta)^{n+\frac{1}{2},**} \nabla \delta\pi \right) = \frac{1}{2} \bar{\nabla} \cdot \left((P\vec{v})^{n+1,**} + (P\vec{v})^n \right). \quad (23)$$

In (22) and (23), $\bar{\nabla}$ and $\bar{\nabla} \cdot$ denote standard finite volume discretizations of the gradient for the primary control volumes and the divergence for node-centered dual cells, respectively. Both are obtained by analytically evaluating the boundary integrals for the respective control volumes. In doing so, we assume piecewise constant data on the primary control volumes for $(P\vec{v})$ and piecewise bilinear distributions for $\delta\pi$. This is also why the second term on the left in (23) includes the exact gradient operator acting on the piecewise bilinear distribution of $\delta\pi$ under the divergence. For $\alpha = 0$ this discretization corresponds to one member of a family of approximate projection schemes, see, e.g., [Almgren et al. \(1996\)](#). There is also an inf-sup-stable exact projection version of the present scheme as documented in [Vater and Klein \(2009\)](#), but that version is not invoked in the tests shown below.

This summarizes the discretization of the model family in (1)–(3) which allows for a continuous “blended” transition between the compressible and pseudo-incompressible models.

3 Control of unbalanced initial acoustic modes

Extensive tests of the scheme described in the previous section, albeit based on using the thermodynamic pressure in the momentum equation rather than Exner pressure, are presented in a recent submission

(Benacchio et al. (2013)), and we do not repeat these here. The present results have been generated with a code that is based on the same discretization approach, except that the predictor step uses directional operator splitting as described in (Klein (2009)) rather than a Runge-Kutta-type time integrator. Let us discuss just one result that highlights a potentially fruitful use of the numerical blend of the full dynamics with an asymptotically balanced model, in this case the pseudo-incompressible dynamics.

Consider a thermal perturbation in a vertical slice $\Omega = [-10, 10] \times [0, 10]$ km², discretized by 160×80 grid points for the runs shown here. We choose a hydrostatically balanced homentropic background atmosphere,

$$p(z) = p_{\text{ref}} \left(1 - \Gamma \frac{g p_{\text{ref}} z}{p_{\text{ref}}} \right)^{\frac{1}{\Gamma}}, \quad (24)$$

$$\rho(z) = \rho_{\text{ref}} \left(\frac{p(z)}{p_{\text{ref}}} \right)^{\frac{1}{\gamma}}, \quad \rho_{\text{ref}} = \frac{p_{\text{ref}}}{RT_{\text{ref}}}, \quad (25)$$

where p_{ref} , g , R , and T_{ref} have the values $1.01325 \cdot 10^5$ N m⁻², 9.81 m s⁻², 287 N m kg⁻¹ K⁻¹, and 300 K, respectively. Then we perturb the potential temperature perturbation as in Klein (2009) by

$$\theta'(x, z) = \begin{cases} \delta\theta \cos^2(\frac{\pi}{2}r) & (r \leq 1) \\ 0 & \text{otherwise} \end{cases}, \quad \begin{aligned} \delta\theta &= 2 \text{ K} \\ r &= 5 \sqrt{(\frac{x}{L})^2 + (\frac{z}{L} - \frac{1}{5})^2} \\ L &= 10 \text{ km} \end{aligned} \quad (26)$$

The initial velocity is zero, and rigid wall boundary conditions on all sides. The overall evolution of the system is visualized in Fig. 1 by several snapshots of vertical velocity and potential temperature.

We observe that the initial data described above include a somewhat naive initialization of the pressure by the hydrostatic background distribution. Since there is a buoyant plume at the center of the domain, this pressure distribution is not balanced in any way. As a consequence, the evolution starting from these initial data will include acoustic perturbations. A short time simulation over 350s using short time steps to resolve the acoustic modes reveals indeed that acoustic oscillations develop in the compressible case, while they are absent in the pseudo-incompressible dynamics. This is seen in the top panel of Fig. 2 which shows the time sequences of Exner pressure increments as computed in the first implicit correction equation (20) at location $(x, z) = (-7.5, 5.0)$ km for the compressible (solid line) and the pseudo-incompressible (dashed line) cases. The middle panel of Fig. 2 shows the same comparison when we run both codes with large advective time steps. The oscillations of the pressure increments from the compressible run are now by about one order of magnitude smaller, showing that the semi-implicit compressible scheme robustly handles large time steps. Yet, the oscillations in the compressible run are still substantial and quite rough in addition.

The bottom panel of Fig. 2 shows again a comparison of pseudo-incompressible and compressible results for the short time step, but here we have followed a ‘‘blending strategy’’ to control the acoustic imbalances, as described first by Benacchio et al. (2013), as follows: The compressible run starts in pseudo-incompressible mode for a couple of time steps, then the compressibility parameter α from (3) is raised linearly in time to reach unity at twice this time interval, and then the simulation continues in the fully compressible mode. For the blended run in the third panel of Fig. 2 only the first time step uses sound-proof dynamics, the second runs at $\alpha = 0.73$, and from the third time step onwards the dynamics is fully compressible. To display the close proximity of the blended and pseudo-incompressible results at the right scale in the graph the first time step, which has a large excursion in $\delta\pi$, has been cut out. Note that the pressure scale in this panel is about three orders of magnitude smaller than in the first one. At this level of resolution, timestep-to-timestep noise with an amplitude of order $1 \cdot 10^{-7}$ becomes visible in the pseudo-incompressible pressure increments. It has been removed here by a simple three-point-filter, $\overline{\delta\pi}_n = (\delta\pi_{n-1} + 2\delta\pi_n + \delta\pi_{n+1})/4$.

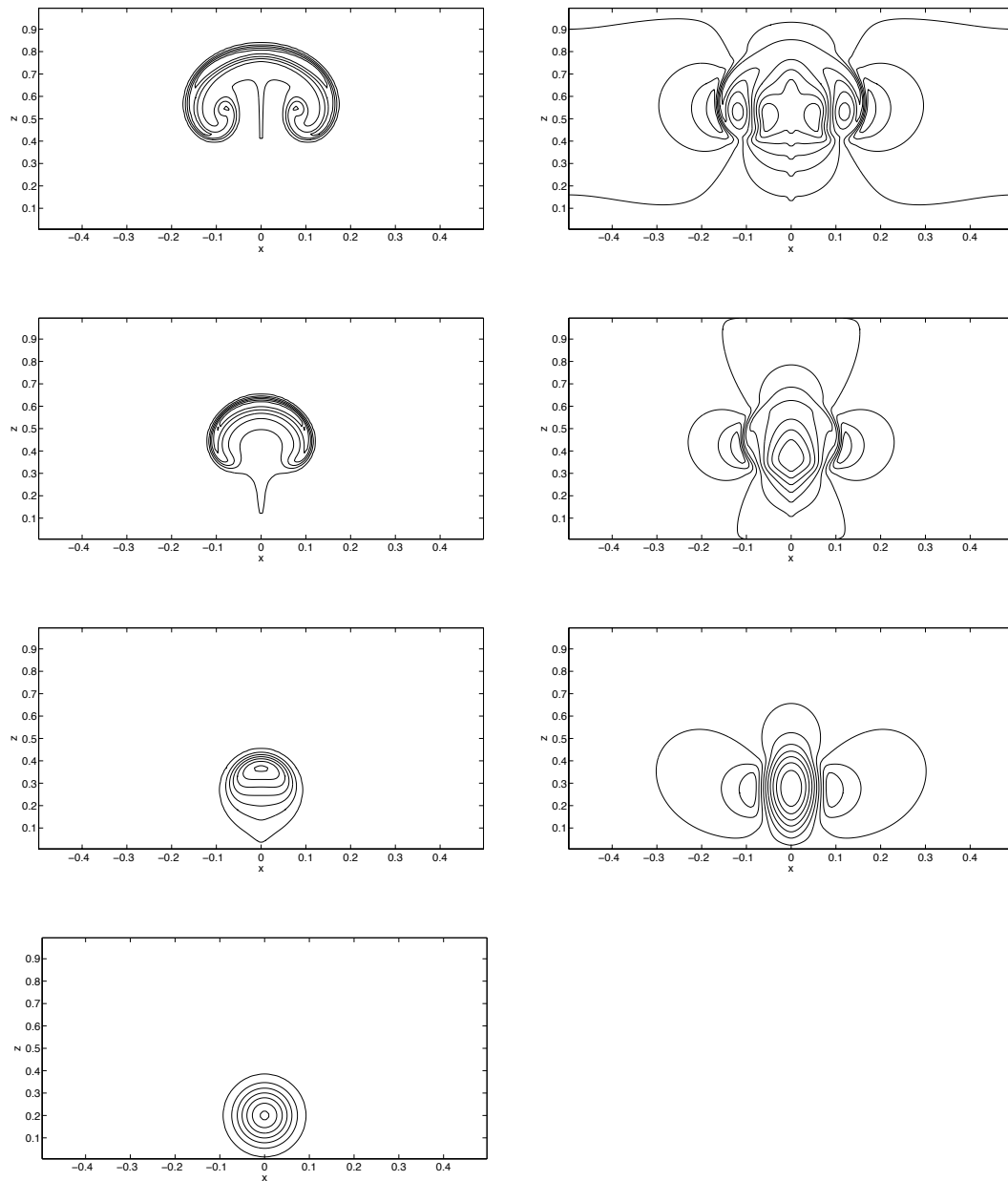


Figure 1: Results from a compressible simulation for the rising bubble test case with initial data from (24)–(26), at $CFL_{adv} = 0.9$, and with 160×80 equally spaced grid cells resolving the domain. Left column, from bottom up: Potential temperature contours at $\theta = (1 + [1, 11, 22, 33, 44, 55, 65] \cdot 10^{-4}) \cdot 300\text{K}$ at times $t = [0, 350, 700, 1050]\text{s}$. Right column, from bottom up: vertical velocity contours at the respective output times, 15 contours between minima and maxima (MatLab `contour()` standard call), with $[w_{min}, w_{max}] = ([-4.1, 9.5], [-8.0, 14.1], [-8.2, 13.2])\text{ms}^{-1}$. These graphs are virtually indistinguishable from those obtained from a pseudo-incompressible run (not shown).

We conclude that a numerical scheme which allows for a continuous transition between full dynamics and a balanced limit model can be used to control imbalances of fast wave dynamics in the initial data essentially without computational overhead. The only potential overhead results from the fact that the Helmholtz problems to be solved for $\alpha > 0$ are better conditioned than the Poisson equations to be solved for $\alpha = 0$. Depending on the linear system solvers used, this may require more iterations for solving the correction equations in the sound-proof setting.

4 Conclusions and discussion

In this paper we consider a family of dynamical flow models that exploits the close structural similarity of the pseudo-incompressible and the full compressible equations to continuously interpolate between these two limiting cases based on a compressibility parameter, $\alpha \in [0, 1]$. All members of the family satisfy a physically meaningful total energy conservation law. A corresponding “blended” compressible/pseudo-incompressible flow solver has recently been proposed by [Benacchio et al. \(2013\)](#) and is summarized here.

The blended scheme is used to demonstrate how acoustically imbalanced initial data from a standard “rising bubble” test case can be balanced straightforwardly by performing a few pseudo-incompressible time steps first, and then increasing the compressibility parameter continuously from zero to one within another few steps. We have demonstrated that even a single pseudo-incompressible and one time step with an intermediate value of α are sufficient to effectively remove the acoustic imbalance.

While one might argue that a similar result could be achieved by just determining the initial pressure for the compressible run from the pressure Poisson equation of the sound-proof model, the present approach has several advantages: (i) the removal of imbalance is achieved without invoking any routines aside from the flow solver itself; (ii) the balancing procedure is guaranteed to minimally distort the flow dynamics as it invokes a limit model that has been shown to be asymptotically close to the full dynamics in terms of the flow Mach number and the potential temperature stratification ([Klein et al. \(2010\)](#)). This latter observation implies that the same procedure of reducing α to zero briefly and then blending back to the compressible dynamics could be invoked productively to remove imbalances in a data assimilation procedure. When, for instance, potential temperature adjustments are introduced in a data assimilation step, they will induce buoyancy perturbations and related acoustic imbalances as in the rising bubble test case discussed above. The blending procedure would remove these imbalances while continuously updating the flow in time.

Thinking ahead, we conjecture that a three-dimensional solver on the sphere can be designed to blend with hydrostatically and with geostrophically balanced models in a similar fashion. The resulting scheme would provide an elegant route to balanced data assimilation in general.

Acknowledgements

The authors thank ECMWF for the invitation to contribute to an exciting seminar, Piotr Smolarkiewicz for critical discussions and encouragement related to this work, and Deutsche Forschungsgemeinschaft for their support through the Berlin Mathematical School, grants KL 611/23-1,2, and the “MetStröm” Priority Research Programm (SPP 1276).

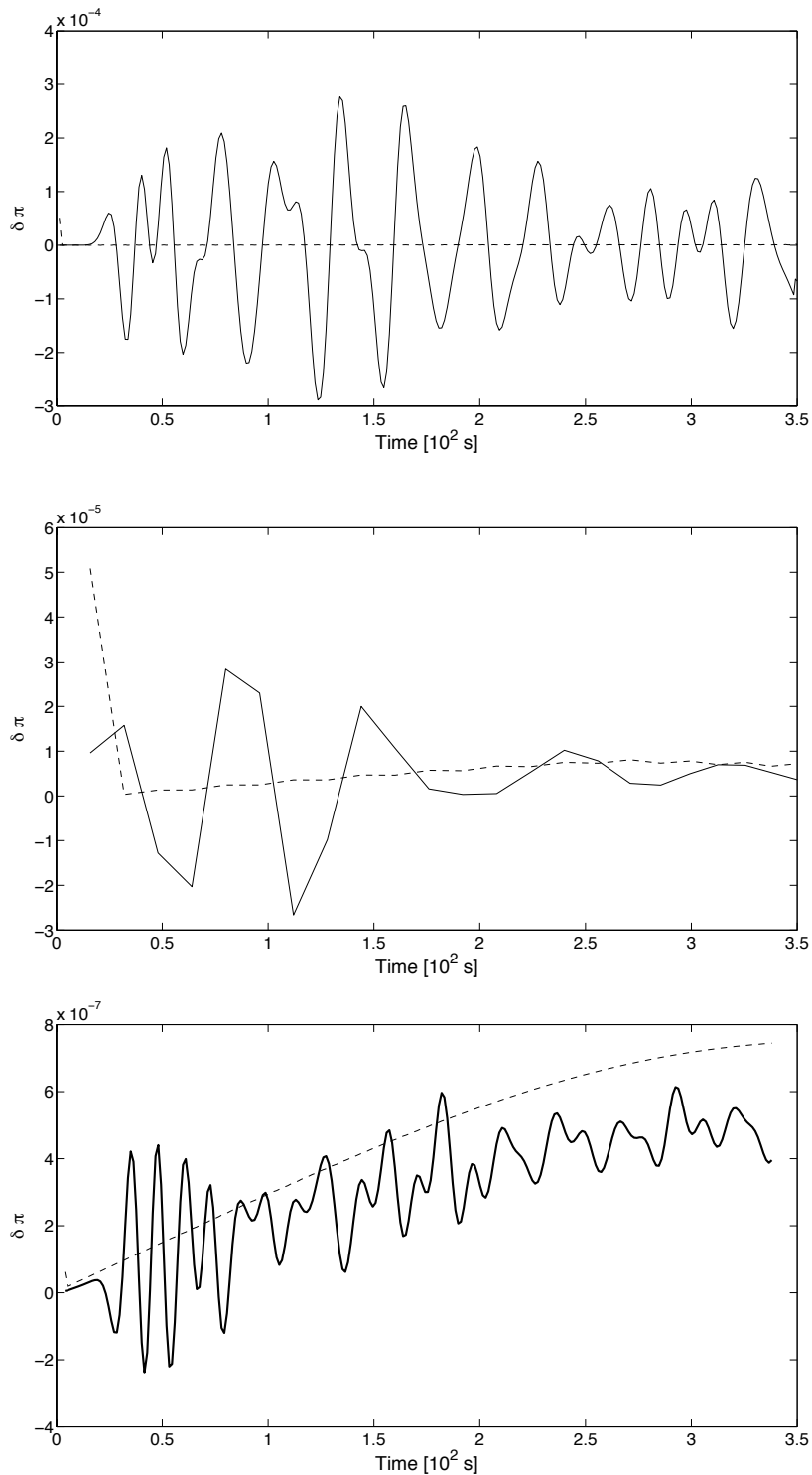


Figure 2: Time sequences of dimensionless cell-centered pressure increments computed in the first Poisson/Helmholtz problem for the rising bubble test case at location $(x, z) = (-7.5, 5.0)$ km. Solid line: compressible model; dashed line: pseudo-incompressible model. Top: time step $\Delta t = 1.3$ s corresponding to $CFL_{ac} < 3.2$ for the entire run; middle: time step $\Delta t \sim 12$ s corresponding to $CFL_{adv} \sim 0.9$; bottom: comparison of pseudo-incompressible (dashed) and blended pseudo-incompressible/compressible (solid) runs, again for time step $\Delta t = 1.3$ s, with data from first time step removed, and step-to-step fluctuations of $\delta\pi$ of amplitude $\sim 1 \cdot 10^{-7}$ in the pseudo-incompressible run filtered by simple 3-point averaging. The first time step in the blended run is pseudo-incompressible, the second operates with $\alpha = 0.733$, and from the third time step onwards the dynamics is fully compressible. Note the different scaling of the vertical axes in all three plots!

References

- Achatz, U., R. Klein, and F. Senf (2010). Gravity Waves, Scale Asymptotics and the Pseudo-Incompressible Equations. *J. Fluid Mech.* 663, 120–147.
- Almgren, A., J. Bell, and W. Szymczak (1996). A numerical method for the incompressible Navier-Stokes equations based on an approximate projection. *SIAM J. Sci. Comput.* 17, 358–369.
- Almgren, A. S., J. B. Bell, C. A. Rendleman, and M. Zingale (2006). Low Mach number modeling of type Ia supernovae. I. Hydrodynamics. *Astrophys. J.* 637, 922–936.
- Bannon, P. R. (1996). On the anelastic approximation for a compressible atmosphere. *J. Atmos. Sci.* 53, 3618–3628.
- Bell, J. B. and D. Marcus (1992). A second-order projection method for variable-density flows. *J. Comput. Phys.* 101, 334–348.
- Benacchio, T., W. O’Neill, and R. Klein (2013). A blended soundproof-to-compressible model for atmospheric dynamics. *Mon. Wea. Rev. (submitted)*, (available upon request from the authors).
- Bijl, H. and P. Wesseling (1998). A unified method for computing incompressible and compressible flows in boundary-fitted coordinates. *J. Comput. Phys.* 141, 153–173.
- Colella, P. and K. Pao (1999). A projection method for low speed flows. *J. Comput. Phys.* 149, 245–269.
- Cullen, M. J. P. (2007). Modelling atmospheric flows. *Acta Numerica* 16, 67–154.
- Durran, D. R. (1989). Improving the anelastic approximation. *J. Atmos. Sci.* 46, 1453–1461.
- Durran, D. R. and P. N. Blossey (2012). Implicit-explicit multistep methods for fast-wave-slow-wave problems. *Mon. Wea. Rev.* 140, 1307–1325.
- Dutton, J. A. and G. H. Fichtl (1969). Approximate equations of motion for gases and liquids. *J. Atmos. Sci.* 47, 1794–1798.
- Gatti-Bono, C. and P. Colella (2006). An anelastic allspeed projection method for gravitationally stratified flows. *J. Comput. Phys.* 216, 589–615.
- Jebens, S., O. Knöth, and R. Weiner (2011). Partially implicit peer methods for the compressible Euler equations. *J. Comput. Phys.* 230, 4955–4974.
- Klein, R. (2000). Asymptotic analyses for atmospheric flows and the construction of asymptotically adaptive numerical methods. *Zeitschr. Angew. Math. Mech.* 80, 765–777.
- Klein, R. (2009). Asymptotics, structure, and integration of sound-proof atmospheric flow equations. *Theor. & Comput. Fluid Dyn.* 23, 161–195.
- Klein, R. (2010). Scale-Dependent Asymptotic Models for Atmospheric Flows. *Ann. Rev. Fluid Mech.* 42, 249–274.
- Klein, R. (2011). On the Regime of Validity of Sound-Proof Model Equations for Atmospheric Flows. In *ECMWF Workshop on Non-Hydrostatic Modelling, November 2010*, <http://www.ecmwf.int/publications/library/do/references/list/201010>.
- Klein, R., U. Achatz, D. Bresch, O. Knio, and P. Smolarkiewicz (2010). Regime of Validity of Sound-Proof Atmospheric Flow Models. *J. Atmos. Sci.* 67, 3226–3237.

- Klein, R. and O. Pauluis (2011). Thermodynamic consistency of a pseudo-incompressible approximation for general equations of state. *J. Atmos. Sci.* 69, 961–968.
- Lipps, F. and R. Hemler (1985). Another look at the scale analysis of deep moist convection. *J. Atmos. Sci.* 42, 1960–1964.
- Minion, M. L. (2003). Higher-order semi-implicit projection methods. In *Numerical Simulations of Incompressible Flows*, pp. 126–140. World Sci Publishing.
- Munz, C.-D., S. Roller, K. Geratz, and R. Klein (2003). The extension of incompressible flow solvers to the weakly compressible regime. *Computers & Fluids* 32, 173–196.
- Ogura, Y. and N. Phillips (1962). Scale analysis for deep and shallow convection in the atmosphere. *J. Atmos. Sci.* 19, 173–179.
- Reich, S. (2006). Linearly implicit time stepping methods for numerical weather prediction. *BIT Numer. Math.* 46(3), 607–616.
- Reisner, J. M., A. Mousseau, A. A. Wyszogrodzki, and D. A. Knoll (2005). An implicitly balanced hurricane model with physics-based preconditioning. *Mon. Wea. Rev.* 133, 1003–1022.
- Restelli, M. and F.-X. Giraldo (2009). A conservative discontinuous Galerkin semi-implicit formulation for the Navier-Stokes equations in nonhydrostatic mesoscale modeling. *SIAM J. Sci. Comput.* 31, 2231–2257.
- Schneider, T., N. Botta, K.-J. Geratz, and R. Klein (1999). Extension of finite volume compressible flow solvers to multi-dimensional, variable density zero Mach number flow. *J. Comput. Phys.* 155, 248–286.
- Smolarkiewicz, P. K., C. Kühnlein, and N. P. Wedi (2013). A unified framework for discrete integrations of soundproof and compressible PDEs of atmospheric dynamics. *J. Comput. Phys.*, submitted.
- Tanguay, M., A. Robert, and R. Laprise (1990). A semi-implicit semi-lagrangian fully compressible regional forecast model. *Mon. Wea. Rev.* 118, 1970–1980.
- Vater, S. and R. Klein (2009). Stability of a projection method for the zero Froude number shallow water equations. *Num. Math.* 113, 123–161.
- Wensch, J., O. Knöth, and A. Galant (2009). Multirate infinitesimal step methods for atmospheric flow simulation. *BIT* 49, 449–473.
- Wicker, L. J. and W. C. Skamarock (2002). Time-splitting methods for elastic models using forward time schemes. *Mon. Wea. Rev.* 130, 2088–2097.